https://doi.org/10.31436/iiumej.v26i1.3238

# A NOVEL INDUCED CURRENT PROTECTION SCHEME FOR LARGE-SCALE SOLAR PHOTOVOLTAIC SYSTEMS USING EARLY STREAMER EMISSIONS

**NURUL 'AINI MOHAMAD ZAKARIA[1*], MOHD NAJIB MOHD HUSSAIN[1], KANENDRA NAIDU VIJYAKUMAR[2], INTAN RAHAYU IBRAHIM[2], NOR SALWA DAMANHURI[2], NUR FADZILAH AHMAD[2]**

*[1]School of Electrical Engineering, College of Engineering, Universiti Teknologi MARA, Cawangan Pulau Pinang, 13500, Permatang Pauh, Penang, Malaysia*
*[2]School of Electrical Engineering, College of Engineering, Universiti Teknologi MARA, 40450 Shah Alam, Malaysia*

**Corresponding author: ainizakaria95@gmail.com*

*(Received: 27 March 2024; Accepted: 30 June 2024; Published online: 10 January 2025)*

***ABSTRACT:*** The reliability and safety of large-scale solar photovoltaic systems (LSSPV) is paramount in harnessing renewable energy sources effectively. Given the increasing adoption of solar energy in Malaysian regions prone to lightning strikes, understanding and enhancing protection mechanisms is imperative. This study investigated an induced current protection system for LSSPV using an early streamer emission (ESE) air terminal in Malaysia. Two systems (ESE and Franklin lightning rod types) were employed in a 50 MWp PV power plant spanning 260 acres and were installed on the lightning arrester to ensure adequate protection. The Franklin rod type comprised 763 pieces and was constructed following the Council of Engineer standards (Thailand) standard. Meanwhile, the ESE lightning rod contained 68 pieces and was built following the NFC17102 standard (France). A 150 kA direct lightning impact was then simulated on the PV power plant using MATLAB/Simulink. Consequently, the ESE lightning protection system (LPS) effectively protected and prevented the lightning strike. The Franklin rod type's shading effects and installation costs (USD 10,026,800 vs. USD 8,026,800) were also more significant than the ESE rod type. These outcomes demonstrated that the ESE LPS was suitable for the PV power plant implementation. The findings of this study could also assist in optimizing the lightning protection technology for large-scale PV power plants.

***ABSTRAK:*** Kebolehpercayaan dan keselamatan sistem fotovoltan suria berskala besar (LSSPV) adalah penting dalam memanfaatkan sumber tenaga boleh diperbaharui dengan berkesan. Memandangkan penggunaan tenaga suria yang semakin meningkat di kawasan Malaysia yang terdedah kepada panahan kilat, pemahaman dan meningkatkan mekanisme perlindungan adalah penting. Kajian ini menyiasat sistem perlindungan arus teraruh untuk LSSPV menggunakan terminal udara pelepasan aliran awal (ESE) di Malaysia. Dua sistem (jenis rod kilat ESE dan rod Franklin) telah digunakan dalam loji kuasa PV 50 MWp seluas 260 ekar dan dipasang pada penangkap kilat untuk memastikan perlindungan yang mencukupi. Jenis rod Franklin terdiri daripada 763 keping dan dibina mengikut piawaian Majlis Jurutera (Thailand). Sementara itu, rod kilat ESE mengandungi 68 keping dan dibina mengikut piawaian NFC17102 (Perancis). Kesan kilat langsung 150 kA kemudiannya disimulasikan pada jana kuasa PV menggunakan MATLAB/Simulink. Akibatnya, sistem perlindungan kilat (LPS) ESE melindungi dan menghalang serangan kilat dengan berkesan. Kesan teduhan dan kos pemasangan (USD 10,026,800 lwn. USD 8,026,800) jenis rod Franklin juga lebih ketara daripada jenis rod ESE. Hasil ini menunjukkan bahawa LPS ESE

https://doi.org/10.31436/iiumej.v26i1.3238

sesuai untuk pelaksanaan jana kuasa PV. Penemuan kajian ini juga boleh membantu dalam mengoptimumkan teknologi perlindungan kilat untuk jana kuasa PV berskala besar.

***KEYWORDS:*** *Early Streamer Emission, Lightning protection, Induced current, Solar Photovoltaic farm, Lightning effect*

# 1. INTRODUCTION

Malaysia is increasingly turning to solar energy to diversify energy sources, reduce reliance on fossil fuels, and promote sustainable development. Notably, the Malaysian government has implemented various programs and measures to encourage the expansion of solar energy. The Feed-in Tariff (FiT) mechanism is the main program, which provides solar energy producers with long-term contracts and enticing tariffs. This mechanism has aided the industry's development and investment in large-scale solar projects [1]. Despite the increasing use of solar energy in Malaysia, several issues are still encountered. These issues include intermittency, energy storage, and grid integration. Nonetheless, the Malaysian solar energy industry is anticipated to continue expanding and contribute to the nation's renewable energy goals through ongoing investments and government support.

Malaysia receives plenty of sunlight throughout the year due to its proximity to the equator. The nation gets a high solar irradiation level, rendering it conducive to producing solar energy. Typically, the solar irradiation of Malaysia from 4 to 5 kWh/m2/day annually makes it a desirable location for solar power generation [2]. Multiple large-scale solar projects have also been established in Malaysia, including grid-connected solar farms and power plants. These initiatives significantly improve the country's energy mix while assisting in lowering greenhouse gas emissions. Meanwhile, the interest in residential and commercial solar installations is rising alongside large-scale initiatives. This outcome is attributed to the Malaysian government promoting the installation of solar panels on rooftops through various incentives, such as the Net Energy Metering (NEM) program. Hence, solar energy enables consumers to decrease their total electricity consumption and potentially sell surplus electricity to the grid through NEM [1].

Malaysia is investing in research and development to enhance solar energy technology and improve efficiency further. Academic institutions and research organizations collaborate with business partners to create inventive solutions, such as advanced solar panels and energy storage systems. Therefore, Malaysia's transition to a cleaner and more sustainable energy system relies significantly on solar energy. This system can enhance energy security, lower carbon emissions, and reduce reliance on fossil fuels [3]. Nonetheless, grid-connected solar PV farm systems are costly due to the expensive equipment (PV modules and inverters). Hence, various studies have utilized different experimental methodologies and data analysis approaches to address these issues [4]. These studies aim to sustain the performance and efficiency of solar PV farms while preventing downtime for the investors, ensuring that they receive a return on their investment over a reasonable period.

Malaysian solar PV farms are usually exposed to direct and indirect lightning strikes due to their construction in an open area, resulting in high induced currents. This scenario occurred in Kuala Ketil Solar PV farm two years ago, when a 50 MW solar PV farm was damaged by lightning. Nevertheless, no official damage data was recorded. Generally, a lightning strike can cause interruption and damage the equipment in a solar PV system [5]. The damage to a grid-connected solar PV system from lightning is influenced by the strike location and the type of lightning protection equipment [6,7]. Additionally, the lightning striking point is inversely

related to the distance of the lightning strike impact [8]. For example, the solar PV farm at Tucson Electric Power in Tucson, Arizona, encountered lightning strikes during its operations, resulting in substantial equipment replacement costs [9]. Hence, direct and indirect lightning strikes can demonstrate significant damage and repair expenses [10,11].

Considering that designers often overlook the necessity of lightning protection systems (LPSs) or underestimate their significance, many solar PV farms are vulnerable to lightning strikes due to insufficient protection systems [12]. The lack of an LPS puts solar PV farms at risk of significant equipment damage and system destruction. Certain designers also overlook that replacing or fixing equipment damaged by a strike can surpass the cost of installing an LPS [13]. Therefore, the design and installation of an LPS for a solar PV farm is necessary. A solar panel mounted on a large surface area is more exposed to intense sunlight, resulting in a higher induced current. Lightning strikes can then cause damage to solar PV farms, leading to significant replacement costs, repair expenses, and inconvenience for electricity consumers. Given that an open area-based solar PV farm increases solar radiation and air humidity, this area is more susceptible to lightning strikes. The correlation between solar radiation, air humidity, and lightning discharge frequency produces these lightning strikes [14].

Numerous studies have investigated a suitable LPS for large-scale solar photovoltaic systems (LSSPV) to prevent interruptions during operations while minimizing the repair and replacement cost of the damaged equipment. The improvement of suitable LPS for LSSPV is still being researched. These studies have primarily examined the lightning protection of a solar PV system either theoretically (using simulation tools) [15,16,17,18] or experimentally (laboratory or field tests). Large-scale solar photovoltaic systems (LSSPVs) are typically vulnerable to damage caused by lightning-induced stroke-induced currents (SICs). These SICs cause harmful voltages and currents in PV arrays, inverters, and other electrical equipment, potentially producing equipment failure, system outages, and safety risks. Hence, current lightning protection measures may not adequately reduce the risk of SICs, necessitating the development of a specific induced current protection system for LSSPVs.

The layout and configuration of LSSPVs involving large areas and complex electrical designs pose challenges for implementing effective induced current protection schemes. Therefore, numerous factors (spacing between solar panels, electrical cable routing, and inverter placements) should be considered to reduce the impact of SICs on system performance and reliability. This study investigated an induced current protection system for LSSPV using an early streamer emission (ESE) air terminal in Malaysia. Two systems (ESE and Franklin lightning rod types) were employed in a 50 MWp PV power plant.

## 2. MATERIALS AND METHODS

### 2.1. Study Area and the Proposed Methodology

This section validates the calculation approach used to obtain design parameters, power results, and plant-associated efficiency to measure plant performance. The modeling of the solar PV system in the MATLAB/Simulink software covering the solar PV modules, solar PV array, inverter, transformer, grid, and cable were discussed in detail. Alternatively, the ESE for LPS was modelled based on the datasheet of the manufacturer for Level III ESE, which was designed for the grid-connected solar PV system. The grid-connected solar PV farm system and ESE implementation were validated by comparing this system to the Franklin Rod-based LPS. Subsequently, the solar PV farm data from a 50 MW solar PV farm in Malaysia was acquired as a reference for the case study. This data included all parameter specifications of the components (power, current, voltage, rating, and size) for the solar PV modules, solar PV

https://doi.org/10.31436/iiumej.v26i1.3238

array, inverter, transformer, grid, and cable. A direct lightning strike was then simulated and applied to the solar PV farm using a lightning amplitude current to measure the voltage and current values at different points. This study also provided recommendations on ESE's appropriate number, rating, and position for protective purposes.

Figure 1 displays the flowchart of this study, while Figure 2 depicts the block diagram of a 50 MW solar PV system without a lightning protection scheme. Figure 3 portrays the current solar PV system study model created using MATLAB. The model consisted primarily of an inductor-capacitor-inductor (LCL) filter, a boost converter, a three-phase inverter with (IGBT), and a PV array model. Moreover, the MATLAB PV array icon was created to produce 50 MW using 34 series-connected modules per string containing 1000 parallel strings. The temperature and the irradiance were also set to 25°C and 1000 W/m$^2$ following the standard test conditions (STC). A boost converter was then employed to increase the variable voltage of the solar panel to a higher and steady (direct current) DC voltage. This converter used voltage feedback to maintain a constant output voltage. The IGBT changed the DC output to an (alternating current) AC output. These IGBT firing pulses were generated using the Sinusoidal Pulse Width Modulation (SPWM) technique, which involved comparing three sinusoidal modulating waves to a triangular carrier wave.

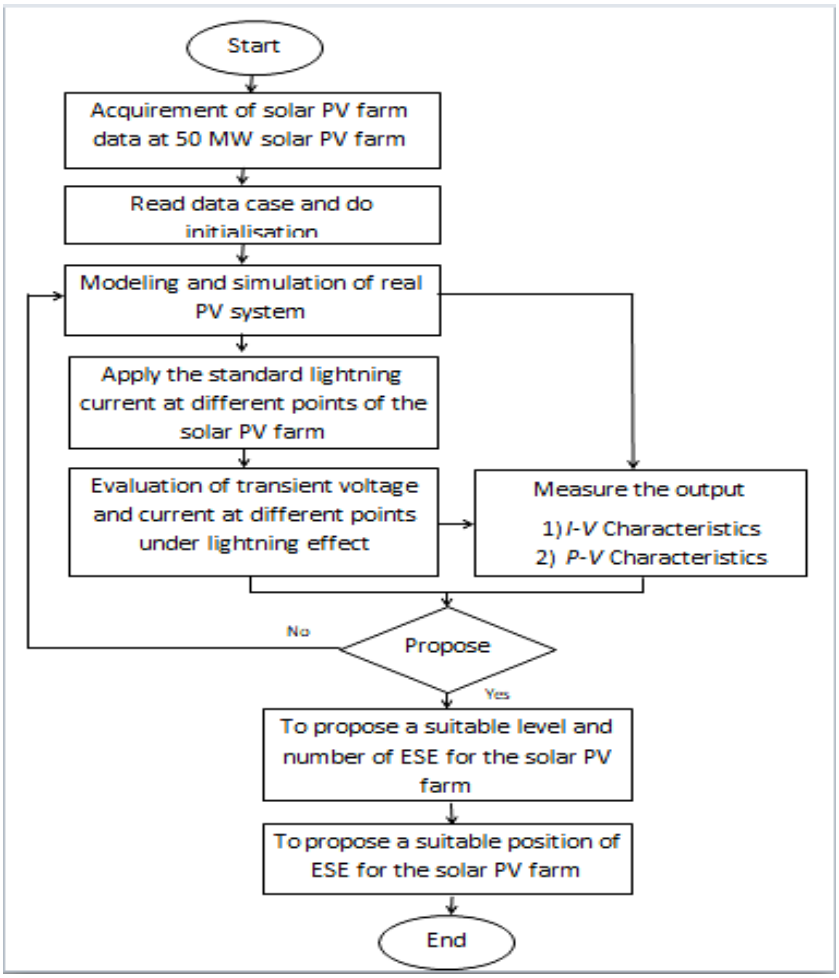


Figure 1. Flowchart of research.

The minimum capacity for the LSS must be 30 MWac to connect to the transmission network. The LSSPV required approval by the Commission at one Interconnection Point [Point of Common Coupling (PCC)] (see Fig. 2). Although a link could be established at any point

https://doi.org/10.31436/iiumej.v26i1.3238

on the grid system to export power generated by the transmission-connected LSS, the power output of an LSS coupled to a gearbox determined its dependency. Likewise, the PV cell employed a series-parallel architecture to establish the basis for simulating solar PV modules. A solar PV array was created by combining these solar PV modules.

The minimum capacity for the LSS must be 30 MWac to connect to the transmission network. The LSSPV required approval by the Commission at one Interconnection Point [Point of Common Coupling (PCC)] (see Figure 2). Although a link could be established at any point on the grid system to export power generated by the transmission-connected LSS, the power output of an LSS coupled to a gearbox determined its dependency. Likewise, the PV cell employed a series-parallel architecture to establish the basis for simulating solar PV modules. A solar PV array was created by combining these solar PV modules.

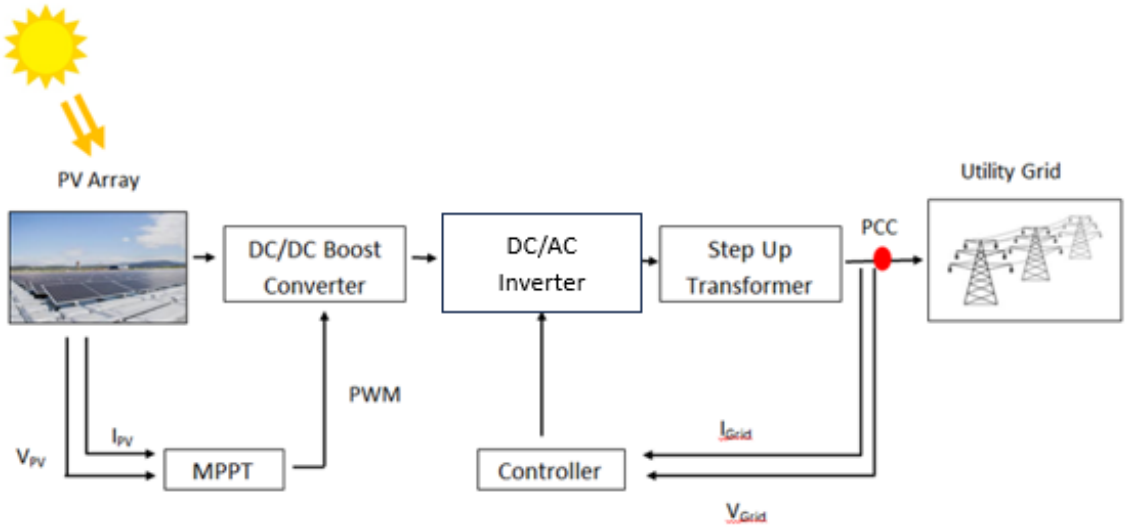


Figure 2. The 50 MW solar farm system block diagram

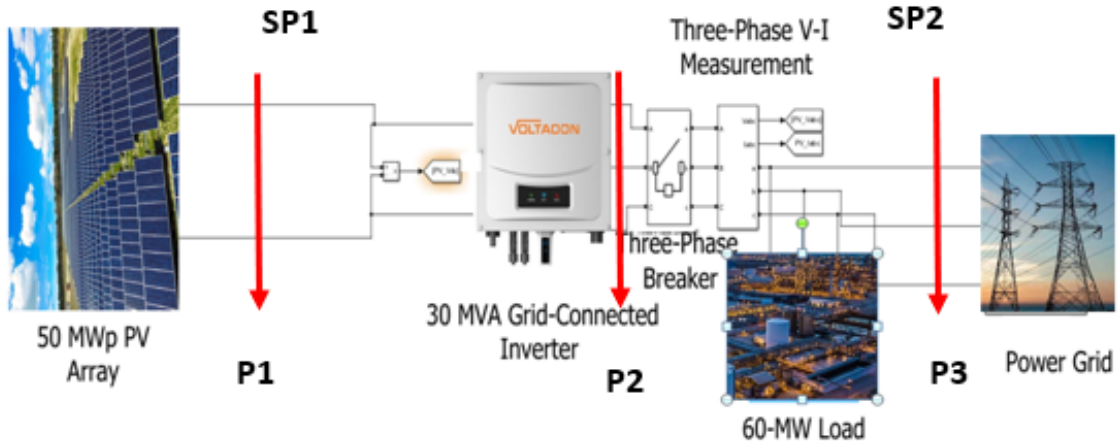


Figure 3. The 50 MW solar farm system

The standard lightning current was applied at different points: the PV array Point 1 (P1), before the inverter Point 2 (P2), and at the utility grid Point 3 (P3). After simulating the PV system, the transient current was examined at these points under the impact of the lightning effect. The measurement output of the current and voltage (I-V) characteristic was then recorded. This study involved creating a highly intricate model of a PV module to examine the correlation between induced current and the solar PV system. The model serves as the

https://doi.org/10.31436/iiumej.v26i1.3238

foundation for electromagnetic simulations replicating the adjacent lightning strike effects on the induced currents in a PV module as follows:

- The location of the lightning strike at different angles concerning the module.
- The current and voltage short circuits between the output terminals of the PV module.
- The interconnections within a four-module array and the functional distinctions between subpar and superior wiring techniques.

### 2.2. Theoretical Background

The grid-connected solar PV farm system was modeled using MATLAB/Simulink based on an actual application solar PV farm (50 MW). The solar PV farm system with a grid connection consisted of solar PV modules, inverters, cables, transformers, and a grid. Before the PV plant design calculations were initiated, suitable PV modules and their corresponding specifications were selected. Thus, the Canadian Solar Inc. CS3U-375P module was chosen for the PV plant design. Table 1 tabulates the main characteristics of these PV modules.

Table 1. Characteristic summary of the proposed PV module

| Parameter | Value |
|---|---|
| Type of Technology | Monocrystalline |
| Maximum open circuit voltage | 47.6 V |
| Maximum short circuit current | 9.93 A |
| Peak power | 375.314 W |

Table 2 lists the details of each component in the solar PV farm modeled in the power systems computer-aided design/electromagnetic transients with DC (PSCAD/EMTDC). Generally, the effectiveness of LPSs (Franklin rods or ESE) mainly depends on their spacing from one another. Therefore, the closer an LPS is placed to the structure it protects, the better it can efficiently redirect the energy from a lightning strike to the ground.

Table 2. A detailed summary of the components in the solar PV farm

| Component | Quantity | Specification |
|---|---|---|
| Solar Module | 136,000 | 72 multi-crystalline solar cells<br>Power solar PV modules = 375 W<br>Voltage of solar PV modules = 47.6 V<br>Current of solar PV modules = 9.93 A |
| Inverter | 100 | Nominal AC Power per inverter = 500 kW |
| Sub Distribution Board (SDB) | 6 | Maximum output aggregated at SDB is 140 kW |
| Main Distribution Board (MSB) | 2 | Maximum output aggregated at MSB is 500 kW |
| Transformer | 1 | 70MVA step-up transformer, 440 V/11 kV |
| Grid | - | 11 kV |

The magnitude of induced currents during a lightning strike largely depended on the separation between LPSs (lightning rods or ESE). Hence, the following are the crucial components:

1. Maximization of lightning protection radius:

   i. The lightning protection radius provided a low-resistance path for the lightning discharge to reach the ground to reduce the likelihood of structural damage.
   ii. To maximize the protected radius, the distance between the LPS and the structure it was protecting must be kept to a minimum. The closer the LPS was to the structure, the better it was at intercepting and safely conducting a lightning strike to the ground.
2. Zone of protection:
   i. The separation distance surrounding the LPS was the protection zone. This system conducted and intercepted lightning strikes within this zone.
   ii. The zone of protection expanded as the separation distance increased. Nonetheless, the LPS and the features of the building should be considered when optimizing this distance.
3. Reduction of induced voltages:
   i. Lightning strikes could change electromagnetic fields, inducing currents and voltages in conductive materials. Thus, an effective LPS minimizes induced voltages.
   ii. Enhancing the overall efficiency of the LPS involved minimizing induced currents and voltages in the protected structure by optimizing the separation distance.
4. Risk of side flashes:
   i. Side flashes could occur when lightning current leaps from the LPS to other conductive pathways (such as metal structures or utilities) due to insufficient separation distance. This process put the occupants of the protected structure in danger.
   ii. Proper separation distances were required to minimize side flashes and ensure that the lightning discharge followed the intended path to the earth.
5. Compliance with standards and guidelines:
   i. Separation distance guidelines for LPSs were included in national and international standards, such as the National Fire Protection Association (NFPA) and the International Electrotechnical Commission (IEC).
   ii. Adhering to these criteria ensured that the separation distance was based on scientific considerations and provided a uniform protection level.

Overall, separation distance primarily affected induced currents by affecting the efficiency of the LPS. Therefore, this distance must be optimized to maximize protection, minimize induced voltages, and lower the occurrences of side flashes during a lightning strike.

### 2.3. LPS Validation and Mathematical Modelling

This section validates the LPSs (ESE and Franklin Rod) using MATLAB/SIMULINK with the manufacturer-provided data. The design process used two systems (conventional and ESE) to define the external lightning concept. Thus, the lightning protection design consisted of the separator distance and air termination system. In contrast, this design neglected the down conductors, earth termination, and lightning equipotential bonding. The validation process is as follows:

1. The (IEC/EN 32305) standard defined the conventional system and was a design reference for three different methods to protect the PV power plant.
2. The angle under the shade concept and the height level of the lightning rod defined the protective angle method. Given that the height level could affect the PV power plant, this parameter must be specified as the separation distance clearance.

https://doi.org/10.31436/iiumej.v26i1.3238

3. The rolling sphere method or electro-geometric model was utilized using the protective angle method to protect PV power plants. The air terminator rod position for installation is determined by expressing a radian of an equation as follows:

$$r = 10 \times I^{0.65} \quad (1)$$

where $I$ is the current strike magnitude, and $r$ is the rolling sphere radian. Alternatively, the four lightning protection classes were connected through the $r$ value calculation. Table 3 summarizes the lightning rod positions computed using the $r$ value.

Table 3. Calculation summary of the lightning radius protection

| Class of Lighting Protection Zone (LPS) | Radius of the Rolling Sphere (r) |
|---|---|
| I | 20 m |
| II | 30 m |
| III | 45 m |
| IV | 60 m |

4. The mesh approach was used to develop lightning protection for a building or infrastructure with a complicated and flat geometry. Therefore, the mesh dimensions defined the mesh method, which was connected to the degree of lightning protection.

5. The French NFC17102 standard on the ESE rods was applied to define the ESE system. This method utilized the rolling sphere concept by including a rolling sphere and an upward streamer to determine the radius measurement. The height then identified the protection radius of the ESE about the surface or region. Table 3 demonstrates the calculation of the protected zone using the following equations:

$$R_p(h) = \sqrt{2rh - h^2 + \Delta(2r + \Delta)}\,; \in \mathrm{h} \geq 5\ \mathrm{m} \quad (2)$$

$$R_p(h) = h \times R_p(5)/5;\ \in 2\mathrm{m} \leq \mathrm{h} \leq 5\ \mathrm{m} \quad (3)$$

where $R_p(h)$ is the rolling sphere radian at a given height, $h$ is the height of the ESE over the protection zone, is the radius of the rolling sphere, $\Delta$ is the earlier upward streamer with a simple rod by adding $\Delta$T that equals $\Delta = \Delta T \times 106$. On the contrary, a new method was proposed to enhance the efficiency of the current measurement output to decrease the induced current in LSSPV. The equation was a combination of Equations (2) with (3), the vertical spacing between the conductor, i.e., Eq. (4), and the height of the conductor, i.e., Eq. (5), as follows:

$$L = 5.08 + 1.814 \times V + \left[\frac{I}{27.8}\right] \quad (4)$$

$$\varphi_n - \varphi_m = R_{ii}I_i + \sum jwL_{ij}I_jV_n = \sum P_{nm}I_{qm} \quad (5)$$

where $R_{ii}$ is the resistance of segment $i$, and $L_{ij}$ and $p_{ij}$ are the inductance and coefficient of potential between segments $i$ and $j$, nodes inductive cell $n$ and inductive cell $m$. Note that lightning return stroke currents contain high-frequency components. The current in a segment at high frequency was not uniformly distributed over its cross-section due to the eddy current effect. Both resistance and internal inductance then varied significantly with frequency. These values could be determined by surface impedance.

Therefore, the new expression of LPS ESE is as follows:

$$ESE = R_p(h) + L + (\phi_n - \phi_m) \quad (6)$$

https://doi.org/10.31436/iiumej.v26i1.3238

where $R_p(h)$ is the lightning protection radius, $L$ is the spacing between a conductor in meters, $(\phi_n - \phi_m)$ is the conductor segment, and $V$ is the system voltage in kV.

Considering that the source current was known, the contribution from the external current source was divided in Eq. (4). The scalar potentials at the center of its two neighboring potential cells ($n$ and $m$) were also denoted by $\phi_n$ and $\phi_m$. Meanwhile, a scalar Green's function $Gq$ could express the scalar potential $\phi$ for a vertical wire.

Table 4. Summary of the IEC/EN 32305 class for various protection levels

| Lightning Radius Protection | | | |
|---|---|---|---|
| **Lightning Protection Level, h (m)** | **1 (D = 20 m)** | **2 (D = 45 m)** | **3 (D = 60 m)** |
| 2 | 32 | 39 | 43 |
| 3 | 48 | 59 | 65 |
| 4 | 64 | 78 | 86 |
| 5 | 79 | 97 | 107 |
| 10 | 79 | 99 | 109 |
| 15 | 80 | 101 | 111 |
| 20 | 80 | 102 | 113 |
| 45 | 80 | 105 | 119 |
| 60 | 80 | 105 | 120 |

## 2.4. The External Lightning Protection Design for the PV Power

This study assessed the field installation connected with the economics of the PV power plant. The power generated by the PV power plant immediately affected solar PV farms. Thus, examining the quantity of conventional and ESE lightning rods was essential to evaluate the ideal circumstances and capital costs. Fig. 4 depicts the PV power plant location in this study, which is within a 50 MW solar PV farm in Malaysia. A polling sphere method was used within the PV power plant area to design the LPS.


Figure 4. The location of the PV power plant in this study at the Kuala Ketil Solar Farm

https://doi.org/10.31436/iiumej.v26i1.3238

# 3. RESULTS

This section analyses the lightning strike effect from various perspectives without any LPS. Typically, a conductor produces a traveling wave of voltage and current related to surge impedance at the speed of light when lightning hits. Therefore, three different measurement points were utilized after the lightning strike: P1 (which was used to determine the transient at solar PV modules), P2 (the transient at the inverter), and P3 (the transient at the transformer) (see Fig. 3). This process identified the traveling waves of the transient voltage and current causing damage to the components of the grid-connected solar PV farm system.

## 3.1. Effect of Different Lightning Striking Point

This section describes the simulation to study the effects of different lightning striking points. Consequently, two points were observed to possess significant possibilities of being struck by lightning in the solar PV farm: between the solar PV array and inverter (SP1) and between the inverter and substation (SP2) (see Fig. 3.). The lightning struck two independent points, first at SP1 and then moving to SP2. Considering that the solar PV farm was installed in an open area, the 150 kA peak current was applied to SP1 and SP2. Tables 5 to 7 tabulate the lightning strike results of these two different points before the LPS implementation.

Table 5. Lightning strike summary at two different points before the LPS implementation at P1

| **Lightning Amplitude (kA)** | **P1 (PV Array)** | |
|---|---|---|
| | **$V_{pv}$ (kV)** | **$I_{pv}$ (kA)** |
| **SP1** | 3.005 | 1.948 |
| **SP2** | 3 | 4.709 |

Table 6. Lightning strike summary at two different points before the LPS implementation at P2

| **Lightning Amplitude (kA)** | **P2 (After Inverter)** | | | | | |
|---|---|---|---|---|---|---|
| | **$V_{in}$ DC (kV)** | | | **$I_{in}$ Dc (kA)** | | |
| | **Phase A** | **Phase B** | **Phase C** | **Phase A** | **Phase B** | **Phase C** |
| **SP1** | -0.02804 | 0.03894 | $-5.328\times10^{-8}$ | $1.4210^{-6}$ | $-1.95210^{-6}$ | $-1.84510^{-5}$ |
| **SP2** | 0 | 0 | 0 | 1.138 | -1.432 | 0 |

Table 7. Lightning strike summary at two different points before the LPS implementation at P3

| **Lightning Amplitude (kA)** | **P3 (Before Transformer)** | | | | | |
|---|---|---|---|---|---|---|
| | **$V_{in}$ DC (kV)** | | | **$I_{in}$ Dc (kA)** | | |
| | **Phase A** | **Phase B** | **Phase C** | **Phase A** | **Phase B** | **Phase C** |
| **SP1** | 0.09867 | 0.03749 | 0.055 | 3.339 | 1.346 | 2.371 |
| **SP2** | 0.01063 | 0.03751 | 0.03376 | -3423 | 1431 | 2287 |

## 3.2. Effect of Different Cable Lengths

The cables chosen for the solar PV farm inverter were crucial, particularly the DC cable length between the solar PV array and the string inverter. Hence, this section analyses the

https://doi.org/10.31436/iiumej.v26i1.3238

impact of lightning strikes on solar PV array and string inverter (DC side) based on various cable lengths. Different cable lengths ranging from 5 to 20 km were set, and the transient voltage and current results were documented (see Tables 8 to 10). The lightning current of 150 kA peak current was also employed in this analysis.

When different cable lengths were applied to connect the solar PV array and the string inverter, voltage and current traveling waves on the AC side were almost similar. Slight differences between the measured voltage and current on the DC side were still observed, specifically in solar PV modules. Thus, the simulation findings demonstrated a higher correlation between the transient voltage and current with higher cable length. Meanwhile, a higher resistivity value of the core material decreased the maximum overvoltage on the cable. This outcome was attributed to an increased attenuation coefficient, causing the voltage peak value of a voltage wave transmitted along the cable to be reduced. Overall, the effect of a lightning strike on different cable lengths in this study could be employed to determine the LPS installation placement. The cable length connecting the solar PV array and the string inverter should be as short as possible to minimize damage to the solar PV modules.

The findings in this section indicated that a lightning surge could cause damage to the solar PV array and inverter, both of which were costly to replace. Therefore, various voltage and current readings behaviors could be monitored at the solar panel (before and after the inverter) and the main panel connected to the grid. These results were useful in facilitating decisions regarding the LPS placement and identifying the relevant ratings aligning with the objectives of this study.

Table 8. Effect of different cable lengths before the LPS implementation at P1

| Cable Length (km) | P1 (PV Array) | |
|---|---|---|
| | $V_{pv}$ (kV) | $I_{pv}$ (kA) |
| **2** | 3.005 | 1.348 |
| **5** | 7.786 | 1.777 |
| **10** | 2.885 | 2.566 |

Table 9. Effect of different cable lengths before the LPS implementation at P2

| Cable Length (km) | P2 (After Inverter) | | | | | |
|---|---|---|---|---|---|---|
| | $V_{in}$ DC (kV) | | | $I_{in}$ Dc (kA) | | |
| | **Phase A** | **Phase B** | **Phase C** | **Phase A** | **Phase B** | **Phase C** |
| **2** | -0.02804 | 0.03894 | $-5.328\times10^{-8}$ | $1.42\times10^{-6}$ | $-1.952\times10^{-6}$ | $-1.845\times10^{-5}$ |
| **5** | -0.02238 | 0.02639 | $-1.043\times10^{-8}$ | $2.08\times10^{-6}$ | $-2.427\times10^{-6}$ | $-3.612\times10^{-6}$ |
| **10** | -0.01928 | 0.02185 | $-5.126\times10^{-9}$ | $1.86\times10^{-6}$ | $-2.984\times10^{-6}$ | $-1.775\times10^{-6}$ |

Table 10. Effect of different cable lengths before the LPS implementation at P3

| Cable Length (km) | P3 (Before Transformer) | | | | | |
|---|---|---|---|---|---|---|
| | $V_{in}$ DC (kV) | | | $I_{in}$ Dc (kA) | | |
| | **Phase A** | **Phase B** | **Phase C** | **Phase A** | **Phase B** | **Phase C** |
| **2** | 0.09867 | 0.03749 | 0.055 | 3.339 | 1.346 | 2.371 |
| **5** | 0.07135 | (-0.0386) | 0.03797 | (-2.115) | 9.112 | 1.343 |
| **10** | 0.06107 | 0.03823 | 0.03815 | (-1.719) | 7.538 | 1.054 |

### 3.3. Protection Scheme for Solar PV Farm

The ESE lightning protection rod type used in the selected PV power plant was designed according to the standard reference. Notably, the distance pole of the ESE lightning protection rod acquired a radius of lightning protection of 45 m Level III. This system was validated using

https://doi.org/10.31436/iiumej.v26i1.3238

another LPS, Franklin Rod protection, which was created to compare its location distance with ESE lightning protection. A MATLAB simulation was then employed to simulate the effects of LPSs on the PV power plants. This study simulated two forms of lightning protection in a 50 MWp PV power plant. The simulation consisted of the ESE and the Franklin lightning protection types. Subsequently, the case study was performed using the grid-connected solar PV farm system implemented in the 50 MW solar PV farm. The lightning struck SP1 (DC side) and then moved to SP2 (AC side) in the grid-connected solar PV farm system. This lightning strike produced a high transient voltage and current to the nearest point.

The LPS model used in this simulation was verified by comparing it with two different LPS types based on the datasheet of the manufacturer. Several parameters were then analyzed, including cable length, LPS placement, and LPS rating. The ESE lightning protection simulation used 68 rods with a height of 10 m. This design was based on Level III for protection according to the NFC17102 standard, in which the distance length of the ESE lightning type was approximately 44.8999 m. Likewise, the Franklin lightning protection simulation utilized 763 rods with a height of 10 m.

### 3.4. Installation of LPS at 50 MW Solar PV System

This section investigates the installation of LPS ESE Level III on the DC and AC side of the solar PV farm, while Franklin Rod is Level IV. Tables 11 to 13 list the current measurements resulting from a lightning strike applied to SP1 and SP2 with installing an ESE system on the DC and AC sides. The lightning strike possessed a peak current of 150 kA and was conducted through a 2 km cable length with ESE conductors at 5 m, 10 m, and 20 m. Meanwhile, Tables 14 to 16 display the current measurements from a lightning strike applied to SP1 and SP2 by installing an ESE on the DC and AC sides. The lightning strike possessed a peak current of 150 kA and involved a 2 km length of wire with Franklin Rod conductors at heights of 5 m, 10 m, and 20 m.

Table 11. Lightning strike at two different points after ESE implementation at P1

| Lightning Amplitude (kA) | P1 (PV Array) | | |
|---|---|---|---|
| | ESE (5m) | ESE (10m) | ESE (20m) |
| SP1 | -2.54 | -2.61 | -2.45 |
| SP2 | 4,6 | 4.6 | 4.6 |

Table 12. Lightning strike at two different points after ESE implementation at P2

| Lightning Amplitude (kA) | P2 (After Inverter) | | | | | | | | |
|---|---|---|---|---|---|---|---|---|---|
| | ESE (5m) | | | ESE (10m) | | | ESE (20m) | | |
| | Phase A | Phase B | Phase C | Phase A | Phase B | Phase C | Phase A | Phase B | Phase C |
| SP1 | 0.000845 | -0.001956 | -0.001763 | $-8.47\times10^{-4}$ | -0.001814 | -0.001908 | 0.000847 | -0.00181 | -0.001913 |
| SP2 | 3.664 | -1432 | -2231 | 3.664 | -1432 | -2231 | 3.664 | -1432 | -2231 |

Table 13. Lightning strike at two different points after ESE implementation at P3

| Lightning Amplitude (kA) | P3 (before Transformer) | | | | | | | | |
|---|---|---|---|---|---|---|---|---|---|
| | ESE (5m) | | | ESE (10m) | | | ESE (20m) | | |
| | Phase A | Phase B | Phase C | Phase A | Phase B | Phase C | Phase A | Phase B | Phase C |
| SP1 | -3.643 | 1.326 | 2.281 | -3.643 | 1.326 | 2.281 | -3.643 | 1.326 | 2.281 |
| SP2 | -3.66 | 1.433 | 2.231 | -3.66 | 1.433 | 2.231 | -3.66 | 1.433 | 2.231 |

https://doi.org/10.31436/iiumej.v26i1.3238

Table 14. Lightning strike summary at two different points after Franklin Rod implementation at P1

| Lightning Amplitude (kA) | P1 (PV Array) | | |
|---|---|---|---|
| | Franklin Rod (5m) | Franklin Rod (10m) | Franklin Rod (20m) |
| **SP1** | -1.100 | -1,747 | -1.539 |
| **SP2** | 4.595 | 4.595 | 4.599 |

Table 15. Lightning strike summary at two different points after Franklin Rod implementation at P2

| Lightning Amplitude (kA) | P2 (After Inverter) | | | | | | | | |
|---|---|---|---|---|---|---|---|---|---|
| | Franklin Rod (5m) | | | Franklin Rod (10m) | | | Franklin Rod (20m) | | |
| | Phase A | Phase B | Phase C | Phase A | Phase B | Phase C | Phase A | Phase B | Phase C |
| **SP1** | 0.002402 | 0.00181 | -0.000899 | 0.002269 | 0.001383 | -0.00769 | 0.002337 | 0.001284 | -0.0007374 |
| **SP2** | 3.664 | -1.432 | -2.231 | 3664 | -1432 | -2.231 | 3.664 | -1.432 | -2.231 |

Table 16. Lightning strike summary at two different points after Franklin Rod implementation at P3

| Lightning Amplitude (kA) | P3 (before Transformer) | | | | | | | | |
|---|---|---|---|---|---|---|---|---|---|
| | Franklin Rod (5m) | | | Franklin Rod (10m) | | | Franklin Rod (20m) | | |
| | Phase A | Phase B | Phase C | Phase A | Phase B | Phase C | Phase A | Phase B | Phase C |
| **SP1** | -3.643 | 1.326 | 2.281 | -3.643 | 1.326 | 2.281 | -3.643 | 1.326 | 2.281 |
| **SP2** | -3.664 | 1.433 | 2.231 | -3.664 | 1.433 | 2.231 | -3.664 | 1.433 | 2.231 |

Tables 17 to 19 summarize the current measurements when a lightning strike is applied to cables of varied lengths, with ESE installations on the DC and AC sides. The lightning strike possessed a 150 kA peak current with 5 m, 10 m, and 20 m height conductors of ESE. Similarly, Tables 20 to 23 tabulate the current measurements when a lightning strike is applied to cables of varied lengths, with ESE on the DC and AC sides. The lightning strike possessed a 150 kA peak current with 5 m, 10 m, and 20 m height conductors of Franklin Rod.

Table 17. Effect of different cable lengths after ESE implementation at P1

| Cable Length (km) | P1 (PV Array) | | |
|---|---|---|---|
| | ESE (5m) | ESE (10m) | ESE (20m) |
| **2** | -2.452 | -2.51 | -2.459 |
| **5** | -2.12 | -2.08 | -2.08 |
| **10** | -2.22 | -2.093 | -2.09 |

Table 18. Effect of different cable lengths after ESE implementation at P2

| Cable Length (km) | P2 (After Inverter) | | | | | | | | |
|---|---|---|---|---|---|---|---|---|---|
| | ESE (5m) | | | ESE (10m) | | | ESE (20m) | | |
| | Phase A ($\times10^{-4}$) | Phase B ($\times10^{-4}$) | Phase C ($\times10^{-4}$) | Phase A ($\times10^{-4}$) | Phase B ($\times10^{-3}$) | Phase C ($\times10^{-3}$) | Phase A ($\times10^{-4}$) | Phase B ($\times10^{-4}$) | Phase C ($\times10^{-3}$) |
| **2** | 8.45 | -18.14 | -19.08 | -8.47 | -1.814 | -1.908 | 8.47 | -18.1 | -1.913 |
| **5** | -8.4467 | -8.4467 | -8.4467 | -8.229 | 1.538 | 2.099 | -8.32 | 1.59 | 2.056 |
| **10** | 7.13 | 7.13 | 7.13 | 6.45 | -1.032 | -2.476 | 6.65 | -1.076 | -2.452 |

https://doi.org/10.31436/iiumej.v26i1.3238

Table 19. Effect of different cable lengths after ESE implementation at P3

| Cable Length (km) | P3 (Before Transformer) | | | | | | | | |
|---|---|---|---|---|---|---|---|---|---|
| | ESE (5m) | | | ESE (10m) | | | ESE (20m) | | |
| | Phase A | Phase B | Phase C | Phase A | Phase B | Phase C | Phase A | Phase B | Phase C |
| **2** | -3.643 | 1.326 | 2.281 | -3.643 | 1.326 | 2.281 | -3.643 | 1.326 | 2.281 |
| **5** | -2.947 | 1.156 | 1.791 | -2.947 | 1.156 | 1.791 | -2.947 | 1.156 | 1.791 |
| **10** | -2.234 | 0.9184 | 1.315 | -2.234 | 0.9184 | 1.315 | -2.234 | 0.9184 | 1.315 |

Table 20. Effect of different cable lengths after ESE implementation at P3

| Cable Length (km) | P3 (Before Transformer) | | | | | | | | |
|---|---|---|---|---|---|---|---|---|---|
| | ESE (5m) | | | ESE (10m) | | | ESE (20m) | | |
| | Phase A | Phase B | Phase C | Phase A | Phase B | Phase C | Phase A | Phase B | Phase C |
| **2** | -3.643 | 1.326 | 2.281 | -3.643 | 1.326 | 2.281 | -3.643 | 1.326 | 2.281 |
| **5** | -2.947 | 1.156 | 1.791 | -2.947 | 1.156 | 1.791 | -2.947 | 1.156 | 1.791 |
| **10** | -2.234 | 0.9184 | 1.315 | -2.234 | 0.9184 | 1.315 | -2.234 | 0.9184 | 1.315 |

Table 21. Effect of different cable lengths after Franklin Rod implementation at P1

| Cable Length (km) | P1 (PV Array) | | |
|---|---|---|---|
| | Franklin Rod (5m) | Franklin Rod (10m) | Franklin Rod (20m) |
| **2** | -1.700 | -1.747 | -1.539 |
| **5** | -1.62 | -1.608 | -1.611 |
| **10** | -1.522 | -1.527 | -1.525 |

Table 22. Effect of different cable lengths after Franklin Rod implementation at P2

| Cable Length (km) | P2 (After Inverter) | | | | | | | | |
|---|---|---|---|---|---|---|---|---|---|
| | Franklin Rod (5m) | | | Franklin Rod (10m) | | | Franklin Rod (20m) | | |
| | Phase A ($\times10^{-4}$) | Phase B ($\times10^{-3}$) | Phase C ($\times10^{-4}$) | Phase A ($\times10^{-4}$) | Phase B ($\times10^{-3}$) | Phase C ($\times10^{-3}$) | Phase A ($\times10^{-4}$) | Phase B ($\times10^{-3}$) | Phase C ($\times10^{-4}$) |
| **2** | 24.02 | 1.81 | -8.99 | 22.69 | 1.383 | -7.69 | 23.37 | 1.284 | -7.374 |
| **5** | -8.4467 | 1.709 | 19.53 | -8.229 | 1.538 | 2.099 | -8.32 | 1.59 | 20.56 |
| **10** | 7.13 | -1.191 | -23.84 | 6.45 | -1.032 | -2.476 | 6.65 | -1.076 | -4.52 |

Table 23. Effect of different cable lengths after Franklin Rod implementation at P3

| Cable length (km) | P3 (Before Transformer) | | | | | | | | |
|---|---|---|---|---|---|---|---|---|---|
| | Franklin Rod (5m) | | | Franklin Rod (10m) | | | Franklin Rod (20m) | | |
| | Phase A | Phase B | Phase C | Phase A | Phase B | Phase C | Phase A | Phase B | Phase C |
| **2** | -3.643 | 1.326 | 2.281 | -3.643 | 1.326 | 2.281 | -3.643 | 1.326 | 2.281 |
| **5** | -2.947 | 1.156 | 1791 | -2.947 | 1.156 | 1.791 | -2.947 | 1.156 | 1.791 |
| **10** | -2.234 | 0.9184 | 1315 | -2.234 | 0.9184 | 1.315 | -2.234 | 0.9184 | 1.315 |

# 4. DISCUSSION

When lightning hits a conductor, it produces a traveling wave of voltage and current related to surge impedance at the speed of light. Therefore, three different points of measurement were used after the lightning strike to identify the traveling waves of the transient voltage and current that can damage the components of the grid-connected solar PV farm system. The three points include P1, which was used to determine the transient at solar PV modules; P2, the transient at the inverter; and P3, the transient at the transformer.

The separation distance between components in LSSPVs could significantly impact induced currents, particularly during lightning or electromagnetic disturbances [6]. Generally, individual solar panels (modules) are arranged in arrays with specific spacing between them. The separation distance between modules can affect the induced currents during lightning strikes or electromagnetic interference. Thus, greater separation between modules reduced the coupling effects between adjacent modules, potentially minimizing induced currents in neighboring modules during transient events [7]. Alternatively, the separation distance between cabling and conduits within a solar PV system also significantly influenced induced currents. Therefore, proper spacing between cables, conduits, and communication signals could reduce electromagnetic interference and induced currents, maintaining system reliability and performance.

The layout and separation distance between equipment and components within a solar PV system significantly influence induced currents. Thus, proper spacing and arrangement of the equipment could help minimize electromagnetic coupling and induced currents between components, ensuring optimal system operation and reliability during transient events.

The ESE type of lightning protection rod was utilized in the chosen PV power plant. The ESE lightning protection rod was created using the standard as a guide. The PV power plant employed the positioning design of the ESE lightning protection rod type. The ESE lightning protection rod's distance pole offers a 45 m Level III radius of lightning protection. The system was validated using another LPS, Franklin Rod protection. The Franklin lightning protection rod type simulation's positioning distance was created to be compared to the ESE lightning protection.

The generated currents diminished rapidly as the distance from the current impulse increased for the cable length. This outcome was anticipated for the short-circuited bypass diodes, in which the induced currents were more significant in the conductive loops closer to the current impulse than those farther away. Specifically, the induced currents for the 2 km and 10 km separation distances increased by 150 kA with the addition of a short-circuit loop between the output terminals of the model. Subsequently, an investigation was conducted using ESE with LPS installation following the accepted practices and standards. The analysis was divided into two cases: LPS ESE Level III and LPS Franklin Rod Level IV. Consequently, LPS ESE Level III was installed with a cable length of 2 km. The length of conductor LPS ESE was also 10 m, sufficient to safeguard the equipment (solar PV modules and string inverters).

Separation distance standards must be followed for PV systems to minimize induced currents, guarantee safety, maximize performance, abide by regulations, and support certification and warranty requirements. By adhering to standard guidelines, PV installations can be designed, installed, and operated with confidence, reducing risks and increasing system reliability.

There are several ways in which separation distance affects induced currents in large-scale solar PV systems. In particular, during lightning events and electromagnetic disturbances,

proper spacing between modules, cables, and electrical components helps to minimize electromagnetic coupling, reduce induced currents, and ensure the safety and reliability of the PV system.

## 5. CONCLUSION

This study successfully compared the simulated installation of LPS ESE and LPS Franklin Rod for lightning protection in a PV power plant. A lightning strike produced high transient voltage and current that could severely damage solar PV modules, inverters, and other electronic components. Therefore, a template model of a grid-connected solar PV farm system was developed to evaluate the LPS. An analysis of the lightning effect on the solar PV farm without any installation of LPS was conducted to study the consequences if the engineers neglected the LPS installation. This analysis was performed based on two crucial perspectives: striking points and different cable lengths. Meanwhile, the new ESE technique was used to replicate the lightning-induced current in the PV system. Consequently, significant induced current was observed, which might potentially damage the PV systems if appropriate protection measures were not implemented. Certain scenarios also demonstrated that the simulated results matched the field observations recorded in other studies.

The PV system's lightning-induced current was simulated using the new ESE technique. Considerable induced current was seen, which could harm the PV systems if proper protective measures were not taken. In certain instances, the simulation resultswere in line with the field observations documented in Tables 11 to 23.

It was discovered that the induced currents quickly attenuate as the distance from the current impulse increases for the length of the cable. As expected, in the case of the short-circuited bypass diodes, the induced currents were higher in the conductive loops that were closer to the current impulse than in the conductive loops that were farther away. For both the 2 km and 10 km separation distances, the induced currents increased by 150 kA by adding a short-circuit loop between the model's output terminals.

Although the LPS Franklin Rod Level IV provided sufficient protection equipment, this system required more rod amounts installation than LPS ESE. The performance of using this LPS Franklin Rod slightly increased, requiring more installation costs. Thus, the LPS ESE Level III was more suitable for a direct lightning strike than the LPS Franklin Rod Level IV. This outcome was attributed to the capability of the LPS ESE Level III to handle the high energy of LPS for solar PV farms for a long duration. Overall, the LPS ESE Level II was required to be installed between electronic parts connected in series for protection from direct lightning strikes

## ACKNOWLEDGEMENT

The authors would like to acknowledge the Journal Support Fund, Universiti Teknologi MARA, for supporting this article.

## REFERENCES

[1] Wong, J., Lim, Y.S., Tang, J.H., and Morris, E. (2014) Grid-connected photovoltaic system in Malaysia: A review on voltage issues. *Renewable and Sustainable Energy Reviews*, *29*, 535–545. https://doi.org/10.1016/j.rser.2013.08.087.

[2] Zhang, P.,Jin,Q. (2022) Evolution, status, and trends of exergy research: a systematic analysis during 1997–2020. *Environ Sci Pollut Res 29*, *30*(2), 73769-73794, https://doi.org/10.1007/s11356-022-22915-y.
[3] Azhari, A.W., Sopian, K., Zaharim, A., and Al Ghoul, M. (2008) A new approach for predicting solar radiation in tropical environment using satellite images - Case study of Malaysia," *WSEAS Transactions on Environment and. Development*, *4*(4), 373–378.
[4] Soares, A.P. (2013) Investigation of Typical Problems of PV-Inverters. *Journal of Chemical Information and Modelling*, *53*(9), 1689–1699.
[5] Shahsavari, A., Farajollahi, M., Stewart, E., Roberts, C., and Mohsenian-Rad, H. (2017, 17-19 September) A data-driven analysis of lightning-initiated contingencies at a distribution grid with a PV farm using Micro-PMU data. North American Power Symposium (NAPS). Morgantown, USA. https://doi.org/10.1109/NAPS.2017.8107307.
[6] Coetzer, K.M., Gideon Wiid, P., and Rix, A.J. (2019, November) Investigating lightning induced currents in photovoltaic modules. *International Symposium on Electromagnetic Compatibility* - EMC Europe, pp 261–266, https://doi.org/10.1109/EMCEurope.2019.8871890.
[7] Ren, H., and Zhang, Y. (2021) Research on induced current and induced voltage of 500 kV double circuit transmission line. *Energy Reports*, *7*(1), 216–223. https://doi.org/10.1016/j.egyr.2021.01.077.
[8] Hernández, J.C., Vidal, P.G., and Jurado, F. (2008) Lightning and surge protection in photovoltaic installations. *IEEE Transactions on Power Delivery*, *23*(4), 1961–1971. https://doi.org/10.1109/TPWRD.2008.917886.
[9] Muller, B., Hardt, L., Armbruster, A., Kiefer, K., and Reise, C. (2015) Yield predictions for photovoltaic power plants: Empirical validation, recent advances and remaining uncertainties. *Progress in Photovoltaics, 24*(4), 570–583, https://doi.org/10.1002/pip.2616.
[10] Belik, M. (2014, 12-14 May) PV panels under lightning conditions. Proceedings of the 2014 15th International Scientific Conference on Electric Power Engineering (EPE), pp. 367–370. https://doi.org/10.1109/EPE.2014.6839446.
[11] Phanthuna, N., Thongchompoo, N., Plangklang, B., and Bhumkittipich, K. (2010, November) Model and experiment for photovoltaic lightning effects. International Conference on Power System Technology (POWERCON), *2*. https://doi.org/10.1109/POWERCON.2010.5666054
[12] Ittarat, S., Hiranvarodom, S., and Plangklang, B. (2013) A computer program for evaluating the risk of lightning impact and for designing the installation of lightning rod protection for photovoltaic system. *Energy Procedia*, *34*, 318–325. https://doi.org/10.1016/j.egypro.2013.06.760.
[13] Sueta, H.E., Mocelin, A., Zilles, R., Obase, P.F., and Boemeisel, E. (2013, 7-11 October) Protection of photovoltaic systems against lightning experimental verifications and techno-economic analysis of protection. 2013 International Symposium on Lightning Protection (XII SIPDA), pp. 354–359, https://doi.org/10.1109/SIPDA.2013.6729233.
[14] Sobolewski, K., and Sobieska, E. (2022) Analysis of the effectiveness of lightning and surge protection in a large solar farm. *71*(2), 523–542. https://doi.org/10.24425/aee.2022.140726.
[15] Radulović, V., Miljanić, Z. (2020). Determination of Effective Protection Distance in Front of Surge Protective Devices in Low Voltage Systems. In: Avdaković, S., Mujčić, A., Mujezinović, A., Uzunović, T., Volić, I. (eds) Advanced Technologies, Systems, and Applications IV - Proceedings of the International Symposium on Innovative and Interdisciplinary Applications of Advanced Technologies (IAT 2019). IAT 2019. Lecture Notes in Networks and Systems, vol 83. Springer, Cham. https://doi.org/10.1007/978-3-030-24986-1_6.
[16] J. He, Z. Yuan, S. Wang, J. Hu, S. Chen, and R. Zeng, (2009) Effective protection distances of low-voltage SPD with different voltage protection levels," *IEEE Transactions on Power Delivery*, *25*(1), 187–195. https://doi.org/10.1109/TPWRD.2009.2035297.
[17] Pons, E., and Tommasini, R. (2013, 6-8 June) Lightning protection of PV systems. *4th International Youth Conference on Energetics (IYCE)*, Hungary, pp. 1–5, https://doi.org/10.1109/IYCE.2013.6604209.
[18] Formisano, A., Petrarca, C., Hernández, J.C., and Munõz-Rodríguez, F.J. (2019) Assessment of induced voltages in common and differential-mode for a PV module due to nearby lightning

strikes. *IET Renewable Power Generation, 13*(8), 1369–1378. https://doi.org/10.1049/iet-rpg.2018.6033.

[19] Ahmad, N.I., Ali, Z., Kadir, M.Z.A.A., Osman, M., Zaini, N.H., and Roslan, M.H. (2021) Analysis of lightning-induced voltages effect with SPD placement for sustainable operation in hybrid solar PV-battery energy storage system. *Sustainability, 13*(12). https://doi.org/10.3390/su13126889.